A Microscopic Information System (MIS) for petrographic analysis

Simone Tarquini[a][*] and Massimiliano Favalli[a]

[a]*Istituto Nazionale di Geofisica e Vulcanologia, Sezione di Pisa, Pisa, 56126, Italy.*

Abstract

The database and visualization facilities of Geographic Information System (GIS) software are employed to support the analysis of rock texture from thin section by image processing. A Microscopic Information System (MIS) is hence obtained. The method is applied to transmitted light images of 137 samples obtained from 8 granitoid rocks. A slide scanner and a mount for crossed polarization are used to acquire the input images. For each thin section 5 collimated RGB images are scanned: 4 under different directions of crossed polarization and 1 without polarization. A grain segmentation procedure, based on two region growing functions is applied. The output is converted to vector format and refined using editing tools in the MIS environment, which enables a straightforward match between the input imagery and the final vectorized texture. GIS software provides optimal management of the MIS database, allowing the cumulative measurement of more than 87 000 grains.

Keywords: Granitoid rocks; Geographic Information System; Image processing; Petrography.

1. Introduction

A great variety of images types are employed in the Earth and planetary sciences, ranging from microscopic scale images of rock samples to continental scale satellite surveys. The instruments developed for different scales of examination are based on various technologies, but in general the common basis is a sensor that records a signal from the target surface to produce an image.

Different types of software have been developed to deal with such signals, ranging from remote sensing to image processing units, but Geographic Information System (GIS) software is particularly flexible, allowing the combined handling and visualization of data in different formats over a wide resolution range (Burrough, 1989, Pareschi et al., 2000). This software has been recently introduced to the study of rock textures at microscopic scale, using transmitted light microscope images. Li et al. (2008) use GIS software for the segmentation and analysis of grain boundaries, presenting a procedure tested on a few samples. Barraud (2006) applies GIS software to refine and analyze the vectorized texture obtained after segmenting transmitted light microscopy images with third party software (ITK, for Image Toolkit, http://www.itk.org). Fernandez et al. (2005) use GIS software to compute shape-fabric parameters and strain factors from grain boundary maps. In this paper we present a system which uses GIS software to manage the analysis of a large collection of thin sections, applying a custom image processing procedure based on region growing algorithms. This system represents a stand-alone, inexpensive tool that can substitute for the microscope itself in performing a preliminary petrographic survey. It also allows for statistical examination of coarse grained rocks which is difficult with regular microscopes. Any geographic reference is absent, hence we prefer to call the obtained Information System "Microscopic" instead of geographic (MIS).

Petrographic analysis of thin sections by transmitted light microscopy is one of the principal methods for rock characterization and classification. Digital image analysis is the process of identifying and quantifying features in a digital image starting from pixel values (Russ, 2002). When applied to transmitted light microscopy images, the aim of image analysis is to quantify the rock composition and texture by measuring parameters such as modal fractions, crystal/grain size

---

[*] Corresponding author at: Istituto Nazionale di Geofisica e Vulcanologia, Sezione di Pisa, Via della Faggiola 32, 56126 Pisa, ITALY. Tel. +39 050 8311932, fax: +39 050 8311942.
E-mail address: tarquini@pi.ingv.it (S. Tarquini)

distributions and crystal/grain shapes. These features result from petrogenetic processes, and their accurate determination is central in the fields of petrology, volcanology or tectonics (e. g. Jerram et al., 2003; Boorman et al., 2004; Higgins, 2006; Trullenque et al., 2006; Williams et al., 2006; Keulen et al., 2007; Fornaciai et al., 2008; Piochi et al., 2008).

Several authors have applied digital image analysis to automate and speed up the quantification of rock texture from transmitted light microscopy images of thin sections (e. g. Armienti et al., 1994; Launeau et al., 1994; Lumbreras and Serrat, 1996; Goodchild and Fueten, 1998; Launeau and Cruden, 1998; Heilbronner, 2000). However, the application of this method to many rocks is hampered by the complexity of related transmitted light microscopy images.

Here we address the problem of digital image analysis of thin sections by applying four approaches: i) the use of a slide scanner to acquire input imagery in transmitted light from thin sections, leaving aside the petrographic microscope (De Keyser, 1999; Armienti and Tarquini, 2002; Boorman et al., 2004); ii) the storage of the resulting images in a GIS-like database structure that is extremely useful to retrieve, browse and analyze a large archive of thin sections; iii) the application of a custom image analysis procedure based on region growing concepts; and iv) the refinement of the regions after raster to vector conversion using GIS software.

2. From Geographic to Microscopic Information System (MIS)

2.1. Thin sections and GIS

Thin section images are often unintentionally handled using a GIS-like concept. When researchers perform localized microanalysis on their samples (e.g. scanning electron microprobe), they often mark the analyzed spots on these images to organize the measurements (Di Vincenzo et al., 2001; Di Vincenzo et al., 2007). A series of localized information arranged on an image in a reference frame, such as a Cartesian X-Y coordinate system, is a type of graphic information system. If we neglect the effect of geographic projections, the difference between this system and a GIS is that the former is referenced to a local coordinate system, while the latter is referenced to a global Earth surface reference system. Once we are aware of this difference, GIS software can be used in an unconventional way to handle a MIS.

2.2. Image analysis and thin sections

One of the basic concepts of image analysis is that there is a direct relationship between pixel values (the color) and specific classes of features. In the case of transmitted light microscopy this relationship is not straightforward. The main reasons are listed below:

i) In non-isotropic minerals the orientation of the indicatrix with respect to the direction of polarization of light affects the birefringence value and in some case the absorption color.

ii) The optical properties of many minerals are modified by incidental factors such as uneven alteration or ion substitution.

iii) Intra-crystalline structures of many minerals often result in complicated patterns (e.g. twinning, cleavage, zoning), leading to an uneven response to light transmission and possibly adding noise to the images.

iv) Slight differences in thin section preparation can substantially influence the transmitted light behavior of minerals.

v) Without using special devices (e.g.Thompson et al., 2001), the petrographic microscope is well suited to human vision but it is not, per se, an accurate system for the quantification of light (Pirard, 2004).

These factors have hampered the determination of reliable spectral signatures for specific minerals in transmitted light microscopy, and automatic image analysis solutions have been devised only for constrained cases: monomineralic rocks or rocks showing easily distinguishable mineral

phases (e.g. Heilbronner, 2000; Armienti and Tarquini, 2002; Perring et al., 2004; Fornaciai et al., 2008; Li et al., 2008). This paper provides a contribution to overcome this limitation for granitoid rocks. In addition, the presented methodology is ideal to deal with coarse grained samples which are difficult to deal with by using a regular microscope or even a macroscope, owing to the complexity to obtain fields of view greater than 1-2 cm.

2.3. The samples

In this study we analyze 137 thin sections obtained from 49 samples of eight different granitoid rocks that are commonly used in the decorative stone industry (Table 1). The most common minerals in the samples are plagioclase, quartz and K-feldspar with minor mafic minerals (mostly biotite and amphiboles).

Table 1

3. The image database

3.1. Image acquisition

Following the idea of De Keyser (1999), we used a slide scanner (Nikon Coolscan II) for image acquisition, along with an in-house mount for scanning under crossed polarized light (Armienti and Tarquini, 2002) (Figure 1). The scanner allows a resolution up to 9.4 µm/pixel. This value is optimal for our rock samples, where the smallest crystals are usually larger than 100 µm in equivalent diameter. This resolution is also very close to that recently attained by using a digital camera coupled with a microscope (Perring et al., 2004; Barraud, 2006; Obara and Kozusnikova, 2007; Smith and Beerman, 2007). The mount is a rectangular frame with three internal slots holding a thin section and two polarizing filters: one below and one above the thin section (Figure 1). One short side of the mount is open, allowing the insertion and removal of the thin section and of the filters. From a sheet of polarizing plastic we cut 4 pairs of filters with mutually orthogonal directions of polarization with an angular spacing of 22.5 degrees (Figure 1d). By substituting these pairs in the slots, images of the thin section are acquired under 4 directions of crossed polarization together with an image without polarization (Figure 2). The acquisition of multiple images leads to a better characterization of the sample (Terribile and FitzPatrick, 1992; Heilbronner and Pauli, 1993; Launeau et al., 1994; Lumbreras and Serrat, 1996; Feuten, 1997; Goodchild and Fueten, 1998; Heilbronner, 2000; Fueten and Goodchild, 2001; Barraud, 2006; Li et al., 2008).

Figure 1 here

Images have been acquired using the software bundled with the scanner. The acquisition takes typically 20 minutes per thin section for matrices of about 2300×3400 pixels. An advantage of this acquisition method is that, unlike standard microscope-based techniques, the entire surface area of the section is scanned at once (about 2.2×3.2 cm); moreover, a slide scanner is inexpensive compared to a microscope. The 5 perfectly collimated RGB images can be viewed as a single 15 channel image (Figure 2) analogous to a multi-spectral satellite image (Terribile and FitzPatrick, 1995). In a satellite image the channels record different wavelengths of radiation captured by the sensor. Here the difference is due to different polarizing filter combinations. This perspective of viewing the imagery is the key that inspires the image analysis procedure described by Launeau et al. (1994) and Terribile and FitzPatrick (1995).

Figure 2 here.

3

3.2. The image repository in GIS environment

For the handling of our petrographic database we use the ArcView GIS 3.2 package. A significant advantage of GIS software compared to image processing units is that the former is designed to handle data in different formats (e.g. raster or vector), while most image processing units work only with images. To store and efficiently retrieve our data we borrow the repository and browsing concept from a GIS database (Tarquini et al., 2007). GIS software is designed to handle large datasets, and to efficiently address subsets belonging to portions of the area, the information layers are usually arranged in small subsets according to a geographic grid (the "reference" grid). For our purpose we build up a reference grid where each feature is linked to a thin section. In this way, all the files belonging to a particular thin section are retrieved and displayed by clicking on the corresponding feature of the reference grid: a useful tip when dealing with large datasets.

The 5 images acquired for each section have a standardized suffix unequivocally identifying the original filter combination. Using this structure, all input items are directly accessible from the reference grid for visualization and/or analysis.

When loaded by GIS software an image is required to have georeferencing information. For the purpose of our MIS the only necessary condition is that all the images scanned from the same thin section have a coherent reference frame, so the initial coregistration is maintained. We simplify the system by setting the lower left corner of all the images to the origin (coordinates 0, 0), and by setting the pixel size to 1 in the X and Y directions. The actual pixel resolution is considered later, when the measurements are carried out. The mount warrants a perfect mechanical stability, hence acquired images are usually coregistrated. To correct occasional misalignments, three user-defined reference points are identified on each image by the user, then affine transformations re-align the images in the same way GIS software aligns geographic images using geo-referenced points.

After image acquisition and storage, our MIS provides computer assisted visual analysis that can substitute the use of the microscope by performing a preliminary thin section survey. This facility in many cases enables instant mineral determination and possibly rock classification. Moreover, the reference grid permits a rapid visual research over a large archive of thin sections, optimizing data handling.

4. Database elaboration

Considering the complexity of the input imagery outlined in section 2.2, the global procedure for texture determination is organized in two stages (detailed in sections 4.1 and 4.2 respectively): in the first stage, automatic image processing segments the input images into a map of regions providing a preliminary result (Figure 3a,b,c); in the second stage, this result is converted into vector format (Barraud, 2006; Li et al., 2008), then is revised using the customized GIS environment and grains are finally assigned to mineral phases (Figure 3d,e,f).

Figure 3 here.

4.1. The automatic image processing

The 15 input bands were analyzed to reduce the correlation of the global signal (Launeau et al., 1994; Higgins, 2006). The three felsic minerals, plagioclase, K-feldspar and quartz, represent, on average, more than 90% of the 137 thin sections. These minerals are colorless in polarized light and display birefringence colors with the same range of gray tones (see Figures 2, 3, 4). Mafic minerals usually display more saturated colors, but in the global evaluation they carry little weight due to their low abundance. The three bands of the input RGB images are strongly correlated, because a gray color means that they have always approximately the same values. Consequently, for the

automatic image processing, we used only the 5 input red bands, without a relevant loss of information.

A novel object segmentation procedure was developed in C++ language, based on region growing methods. The resultant functions are embedded in the GIS environment using Avenue^{TM} scripts that run the executable via a command line. The basic concept of the region growing method is the detection of relatively homogeneous areas. High frequency information is therefore counterproductive and the input images are cleaned applying a median filter followed by an opening-closing sequence (Russ, 2002) prior to the region growing algorithm. This process acts as both a noise-reduction and low-pass filter that attenuates micro-fractures and cleavages (Figure 4, rows 1-2).

The segmentation procedure was devised by considering the two most recurrent color patterns (p_x) observed in the intra-crystalline textures of the studied samples: p_1 is a gently varying shading (e.g. the color pattern originated by undulose extinction in quartz grains), and p_2 is a quasi-bimodal distributions of pixels values (e.g. the color pattern originated by polysynthetic twinning in plagioclase grains, see Figures 3, 4 and 5). An unseeded region growing function f_g works on the color gradient to deal with p_1 (details in Appendix A), and a seeded region growing function f_d works on color distance to account for p_2 (details in Appendix B). The global procedure starts with a loop that triggers f_g at all the image pixels, giving the preliminary region maps of row 3 in Figure 4. These regions are subsequently broadened using f_d, resulting in the maps of row 4 (Figure 4).

The automatic segmentation does not attribute all the pixels to regions, but unclassified areas are enclosed by classified areas and they are usually well defined by their property of being unclassified; some grains are simply identified by a single unclassified area (see Figure 4). Figure 4 shows 8 representative cases of minerals and textures of the investigated samples. Columns a to d displays cases where f_g is very effective in segmenting patterns such as undulose extinction in quartz (columns a-b), shaded extinction in K-feldspar (column c) or a more straightforward texture as in column d. Columns e to h show cases where f_d helps when f_g fails to classify a relevant portion of the matrix. These are the examples of more complex intra-crystalline color patterns such as perthitic intergrowth (column e) or microcline twinning (column f) in K-feldspar, polysynthetic twinning in plagioclase (column g), or strongly altered plagioclase (columns e to h) possibly combined with strong zoning (column h).

Figure 4 here.

4.2. Vector texture

Results of the automated image processing procedure are transformed from raster to vector format (Barraud, 2006; Li et al., 2008). The methods described in section 3.2 provide an effective and user-friendly comparison between the vectorized texture and the input images (see also Figures 3 and 4). The user can therefore easily recognize where the automatic result produces an oversegmentation or an undersegmentation, and can identify the regions that must be merged or split to obtain the actual grains (Barraud, 2006). f_d and f_g were tuned to obtain oversegmentation rather than undersegmentation, because the correction of oversegmentation is easiest. ArcView editing tools were developed to simplify and speed up manual editing of the vector texture. These tools allow merging/splitting of polygons and the attribution of polygons to specific mineral phases. An ideal result of the image processing algorithm would be the exact reproduction of a manually traced texture. A perfect tuning of a few specific cases is possible, but it can likely hamper the application of the system to different samples. A good compromise is the separation of tasks by assigning the most difficult one to the machine (i.e., the recognition of the majority of grain boundaries in the raster domain) and planning manual refinement of the result using an efficient working environment (i.e., the effective editing and visualization tools of the MIS). Manual refinement ensures accurate results (Heilbronner, 2000).

Figure 5 here.

Figure 6 here.

For each thin section, the user defines the extent of a region of interest (ROI) where editing is carried out. For statistical significance, the ROI should include at least 400 grains and is automatically centered in the middle of the thin section.

It is noteworthy that, despite the typical oversegmentation, the real grain boundary contours are almost completely present in the automatic result; only a fraction of the real contours are missing and can subsequently be introduced manually by the user (Table 2). The vector format is ideally suited for the storage of the information on the area, perimeter and mineral phase of all features. Once the editing session is completed, the analysis is finalized by carrying out measurements of the determined grains inside the ROIs. To assess the chosen ROI extent, the measured mode is plotted vs the ROI size (Figure 6), and when the mode becomes stable, the ROI extent is accepted. All the performed measurements are stored according to the same repository structure described for the images, hence the results can be retrieved and displayed using the reference grid (e.g, Figure 7).

For every rock the crystal size distribution is derived (Higgins, 2000). Table 2 reports statistics of the modal analyses. 87,064 grains were identified within the 137 analyzed thin sections (on average more than 600 per thin section). The average cumulative length of grain boundaries automatically detected for each section is about 1.6 m while the hand traced grain boundaries are about 7 mm per thin section. The columns Kf_r, Pl_r and Qz_r report the ratios between the regions and the actual grains for felsic minerals.

Table 2 here.

4.3. Sample processing time

To evaluate the effectiveness of the database processing we quantify the duration of the global procedure; that is the CPU-time for the automatic batch processing, and the operator-time for the manual vector editing. We worked on a Pentium 3 2.2 GHz CPU. The CPU-time depends on the number of pixels in the input images and on the number of determined regions. 1-1.5 hours of CPU time per thin section is required for the studied samples.

Quantification of the duration of the manual editing session is less straightforward. In general, this parameter depends on three factors: the total number of grains that must be checked, the average quality of the determined regions (the more accurate this result the faster the editing) and the ease of visual mineral phase determination using the MIS facilities. An editing time between 5 and 20 min per cm^2 of thin section is required for the studied rocks. Depending on the rock grain size, a ROI between 1.5 and 4 cm^2 was selected for manual editing.

4.4. Mode errors

Analytical errors in modal analysis are commonly classified as i) sampling errors, linked to the statistical significance of the analyzed sample, ii) measurement errors, due to miscalculation in counting areas, and iii) accidental errors, due to human factors in assigning mineral phases to grains (Chayes, 1956).

In this study the sampling error has been addressed by determining the ROI extent vs mode (Figure 6). Further statistical analyses are beyond the scope of this paper. The measurement error is null if unbiased procedures are written for measurements. The accidental error is low if the visualization capabilities of the MIS allow robust mineral phase determination. It is well known that the attribution of grains to minerals is not always straightforward even using standard microscopy, and greatly relies upon the skill of the petrographer. By comparing our method to the point counting analysis we found that operator errors are similar.

A small proportion of polygons inside the ROIs are not determined, because their size hampers reliable phase attribution (e.g., white regions in Figure 3f and row 5 in Figure 4). The average undetermined area percent (A_u) inside the ROIs is 3.1 (Table 2, last column). The analyzed rocks

contain at least four mineral phases. Assuming that the undetermined areas account for the contribution of all the phases i, proportionally to the measured mode m_i, the error can be calculated for each i phase as $A_u \times m_i$.

5. Concluding remarks

The presented methodology constitutes a Microscopic Information System (MIS) which can substitute for a standard petrographic microscope in carrying out preliminary thin section analysis. Beyond this case, other MIS constituted by different kinds of images can be defined: another image acquisition device and/or another image processing unit can be used maintaining the general structure and functions of the MIS. The reference grid optimizes handling of large thin-section databases and is ideal for applying a database query on the basis of modal or textural parameters. The result of the queries can be instantaneously retrieved and displayed, facilitating the interpretation of data and/or inspiring further analysis. The MIS is also a suitable tool with which to arrange a didactic collection of thin sections, or to store a comprehensive database of all the analyses of a petrographic laboratory.

The presented region growing segmentation procedure proved to be an effective tool for the analysis of 137 thin sections from eight granitoid rocks. This algorithm showed an excellent exportability; once tuned on a granite, it has been successfully applied to all the studied samples without further tuning.

The use of a MIS provides a means for multi scale analysis of rock textures, GIS software being ideally suited to combine the information derived by different sources at different scales on the same sample. As an example the information acquired from a thin section with a standard microscope and electron microscope images could be fruitfully combined.

Appendix A: The Region Growing Function f_g

We define our pixel connectivity as follows: every square pixel shares one side with 4 pixels and a corner with an additional 4 pixels, these 8 neighboring pixels are connected with the central one.

f_g is an unseeded function triggered at every image pixel p_i that can work on an arbitrary number of bands n. The region grows from the starting pixel p_i outwards and then from the edge pixels of the growing area outwards. For every edge pixel f_g computes the Euclidean color distance in the n-dimensional space between this edge pixel and every connected free pixel. A pixel is free if it is not yet assigned to a region. If this color distance is lower than a fixed threshold t_g, then the free pixel is added to the growing region, else the propagation from that edge pixel towards this connection is stopped. The ith (i.e. on p_i) run of f_g stops when all the edge pixels are dammed by t_g. The threshold t_g is a key value: comparing watershed segmentation to region growing, too low a threshold generates an undersegmentation and too high a threshold generates an oversegmentation in the sense of Barraud (2006). The best value is a t_g that provides a minimum number of regions without an excessive merging of actual grains. For our granitoid rocks $t_g = 4.1$ is adequate. When a single spreading process ends, if the region is greater than a fixed number of pixels n_p, this area is stored as a region, otherwise the loop skips to the next pixel. The threshold n_p automatically discards the segmentation of too small grains. For our samples $n_p = 150$ is optimal.

Appendix B: The Region Growing Function f_d

The seeded region growing function f_d, takes as seeds s all the regions already determined by f_g. f_d works on an arbitrary number of bands n as follows:

i. Starting from the pixels inside the ith seed s_i, f_d computes the best bimodal distribution in the n-dimensional space. This step determines two points (colors) in the n-dimensional space.

ii. f_d computes the Euclidean distance in the n-dimensional space between the free pixels connected to the growing s_i and the n-dimensional segment connecting the two points above. If this distance is lower than a fixed threshold t_d, we add the pixel to s_i. This step is repeated until all the edge pixels of the growing s_i are dammed.

Experimentation showed that in our case $t_d = 40$ is adequate.

Acknowledgments

References

Armienti, P., Pareschi, M.T., Innocenti, F., Pompilio, M., 1994. Effects of magma storage and ascent on the kinetics of crystal growth. The case of the 1991-92 eruption. Contributions to Mineralogy and Petrology 115, 402–414.

Armienti, P., Tarquini S., 2002. Power law olivine crystal size distributions in lithospheric mantle xenoliths. Lithos 65, 273–285.

Barraud, J., 2006. The use of watershed segmentation and GIS software for textural analysis of thin sections. Journal of Volcanology and Geothermal Research 154, 17–33.

Boorman, S., Boudreau A.E., Kruger, F.J., 2004. The lower zone–critical zone transition of the Bushveld complex: a quantitative textural study. Journal of Petrology 45, 1209–1235.

Burrough, P.A., 1989. Principles of Geographical Information Systems for Land Resources Assessment. Clarendon Press, Oxford, 194 pp.

Chayes, F., 1956. Petrographic modal analysis. John Wiley and Sons, New Jork, 113 pp.

De Keyser, T.L., 1999. Digital scanning of thin sections and peels. Journal of Sedimentary Research 69, 962–964.

Di Vincenzo, G., Ghiribelli, B., Giorgetti, G., Palmeri, R., 2001. Evidence of a close link between petrology and isotope records: constraints from SEM, EMP, TEM and in situ 40Ar–39Ar laser analyses on multiple generations of white micas (Lanterman Range, Antarctica). Earth and Planetary Science Letters 192, 389–405.

Di Vincenzo, G., Talarico, F., Kleinschmidt, G., 2007. An 40Ar–39Ar investigation of the Mertz Glacier area (George V Land, Antarctica): Implications for the Ross Orogen–East Antarctic Craton relationship and Gondwana reconstructions. Precambrian Research 152, 93–118

Fernandez, F.J., Menendez-Duarte, R., Aller, J., Bastida, F., 2005. Application of geographical information systems to shape-fabric analysis. In: High-Strain Zones: Structure and Physical Properties, 245. Edited by D. Bruhn and L. Burlini, Geological Society of London Special Publication, 409–420.

Fornaciai, A., Landi, P., Armienti, P., 2008. Dissolution/crystallization kinetics recorded in the 2002-2003 lavas of Stromboli (Italy). Bulletin of Volcanlogy, DOI: 10.1007/s00445-008-0249-3.

Fueten, F., 1997. A computer controlled rotating polarizer stage for the petrographic microscope. Computers & Geosciences 23, 203–208.

Fueten, F., Goodchild, J.S., 2001. Quartz C-axes orientation determination using the rotating polarizer microscope. Journal of Structural Geology 23, 895–902.

Goodchild, J.S., Fueten, F., 1998. Edge detection in petrographic images using the rotating polarizer stage. Computers & Geosciences 24, 745–751.

Jerram, D.A., Cheadle, M.J., Philpotts, A.R., 2003. Quantifying the building blocks of igneous rocks: are clustered crystal frameworks the foundation? Journal of Petrology 44, 2033–2051.

Heilbronner, R., 2000. Automatic grain boundary detection and grain size analysis using polarization micrographs or orientation images. Journal of Structural Geology 22, 969–981.

Heilbronner, R.P., Pauli, C., 1993. Integrated spatial and orientation analysis of quartz c-axes by computer aided microscopy. Journal of Structural Geology 15, 369–382.

Higgins, M.D., 2000. Measurement of Crystal Size Distributions. American Mineralogist 85, 1105–1116.

Higgins, M.D., 2006. Quantitative textural measurements in igneous and metamorphic petrology. Cambridge University Press, Cambridge, 270 pp.

Keulen, N., Heilbronner, R., Stuntz, H., Boullier, A.M., Ito, H., 2007. Grain size distribution of fault rocks: A comparison between experimentally and naturally deformed granitoids. Journal of Structural Geology 29, 1282–1300.

Launeau, P., Cruden, A.R., Bouchez, J.L., 1994. Mineral recognition in digital images of rocks: a new approach using multichannel classification. Canadian Mineralogist 32, 919–933.

Launeau, P., Cruden, A.R., 1998. Magmatic fabric acquisition mechanisms in a syenite: Results of a combined anisotropy of magnetic susceptibility and image analysis study. Journal of Geophysical Research 103, 5067–5089.

Li, Y., Onasch, M.C., Guo, Y., 2008. GIS-based detection of grain boundaries. Journal of Structural Geology 30, 431–443.

Lumbreras, F., Serrat, J., 1996. Segmentation of petrographical images of marbles. Computers & Geosciences 22, 547–558.

Pareschi, M.T., Cavarra, L., Favalli, M., Giannini, F., Meriggi, A., 2000. GIS and volcanic risk management. Natural Hazards 21, 361–379.

Perring, C.S., Barnes, S.J., Verrall, M., Hill R.E.T., 2004. Using automated digital analysis to provide quantitative petrographic data on olivine-phyric basalts. Computers & Geosciences 30, 183–195.

Piochi, M., Polacci, M., De Astis, G., Zanetti, A., Mangiacapra, A., Vannucci R., Giordano, D., 2008. Texture and composition of pumices and scoriae from the Campi Flegrei caldera (Italy): implications on the dynamic of explosive eruptions. Geochemistry, Geophysics and Geosystems 9. Q 03013, doi:10.1029/2007GC001746.

Pirard, E., 2004. Multispectral imaging of ore minerals in optical microscopy. Mineralogical Magazine 68, 323–333.

Russ, J.C., 2002. Computer assisted microscopy: the measurement and analysis of images. Plenum Press, New York, 453 pp.

Obara, B., Kozusnikova, A., 2007. Utilisation of the image analysis method for the detection of the morphological anisotropy of calcite grains in marble. Computational Geoscience 11, 275–281.

Smith, J.V., Beermanm E., 2007. Image analysis of plagioclase crystals in rock thin sections using gray level homogeneity recognition of discrete areas. Computers & Geosciences 33, 335–356.

Tarquini, S., Isola, I., Favalli, M., Mazzarini, F., Bisson, M., Pareschi, M.T., Boschi, E., 2007. TINITALY/01: a new Triangular Irregular Network of Italy. Annals of Geophysics 50, 407–425.

Terribile, F., FitzPatrick, E.A., 1992. The application of multilayer digital image-processing techniques to the description of soil thin sections. Geoderma 55, 159–174.

Terribile, F., FitzPatrick, E.A., 1995. The application of some image-analysis techniques to recognition of soil micromorphological features. European Journal of Soil Science 46, 29–45.

Thompson, S., Fueten, F., Bockus, D., 2001. Mineral identification using artificial neural networks and the rotating polarizer stage. Computers & Geosciences 27 (9), 1081–1089.

Trullenque, G., Kunze, K., Heilbronne, R., Stünitz, H., Schmid, S.M., 2006. Microfabrics of calcite ultramylonites as records of coaxial and non-coaxial deformation kinematics: Examples from the Rocher de l'Yret shear zone (Western Alps). Tectonophysics 424, 69–97.

Williams, E., Boudreau, A.E., Boorman, S., Kruger, F.J., 2006. Textures of othopyroxenites from the Burgersfort bulge of the eastern Bushveld Complex, Republic of South Africa. Contributions to Mineralogy and Petrology 151, 480–492

Figure 1. The mount used for scanning thin sections under different polarization conditions. a) Insertion of the thin section. b) Insertion of two polarizers. c) The mount holding a thin section and the polarizers. d) The four pairs of polarizers with mutually orthogonal direction of light polarization. Thin red arrows show the direction of polarization.

Figure 2. An example of the 5 input images. In a corner of each image, the RGB channels are shown separately. The global input imagery consists of 15 perfectly coregistrated bands, 8 bit each. These images refer to the monzo-granite *Grigio sardo* (see Tables 1 and 2)

Figure 3 Sub-images a) to c) show three steps of the automatic image analysis procedure: a) one of the input crossed polarized images; b) the output after automatic image segmentation based on Region Growing algorithms; c) the same output as b, after raster to vector conversion, overlaid on the original image (a). Sub-images d) to f) show the refinement of the automatic output to obtain the final texture (d); the red contours are removed by merging polygons (regions) keeping only the green ones; e) the green contours, identified by the user as the actual grain boundaries. Most of the final grain boundaries already exist, while a few ones have been introduced by the user; f) the final texture, where most of the identified grains have been attributed to a mineral phase (yellow = K-feldspar, magenta = plagioclase, orange = quartz and blue = femics, white = unclassified regions). These images refer to the monzo-granite *Lanhelin* (see Tables 1 and 2). The yellow bar is 2 mm.

Figure 4. Images are arranged in six rows and eight columns identified by numbers and letters respectively. Each column, from top to bottom, displays six steps of the texture determination. The rows represent: 1) an input crossed polarized image; 2) the same image after preliminary filtering; 3) regions obtained by f_g; 4) regions obtained by f_d; 5) final result. The legend for the mineral phases is as in figure 3f; 6, final result overlain to the original image (row 1). The yellow bar is 2 mm. Columns a and c refer to *Yellow topazio*; columns b, e and h refer to *Grigio sardo*; column d refers to *Desert cream*; columns f and g refer to *Silver cloud* (see Table 1 and 2).

Figure 5. Distributions of the values of the red bands (R_v) calculated for a polysynthetic twinned plagioclase (above) and for a microcline twinned k-feldspar (below). Distributions have been calculated in the red box of figure 5g1 (plagioclase) and 5f1 (k-feldspar).

Figure 6. Mode values measured inside the ROI vs ROI extent (mm^2) for quartz, plagioclase, K-feldspar and mafic minerals (respectively Qz, Pl, Kf and Fm). The mode is calculated by averaging the measurements performed on the 30 thin sections of the same rock (Barre gray granite, see Tables 1 and 2 and Figure 7).

Figure 7. Pie diagrams representing the measured mode of 90 (out of 137) thin sections linked to the reference grid. The legend for mineral phases of the pie diagrams is as in Figure 3f. Pie diagrams allow for rapid visual check on the consistency of data between thin sections.
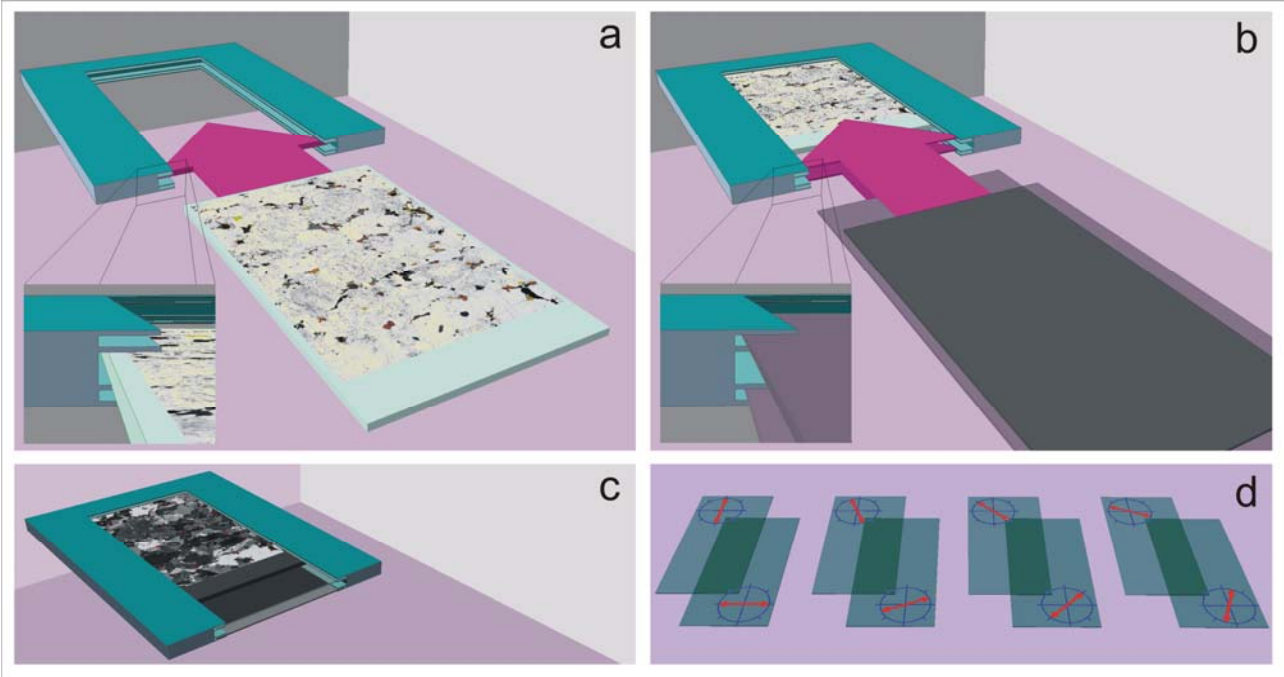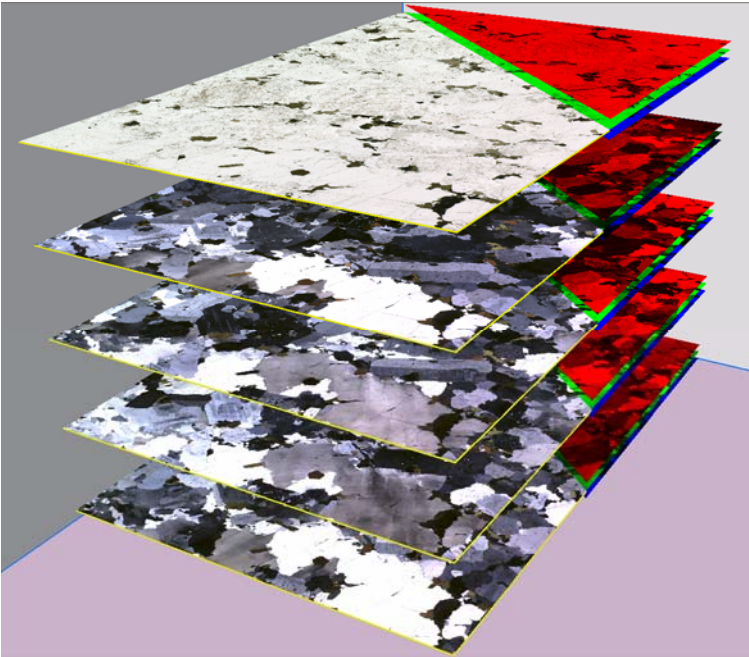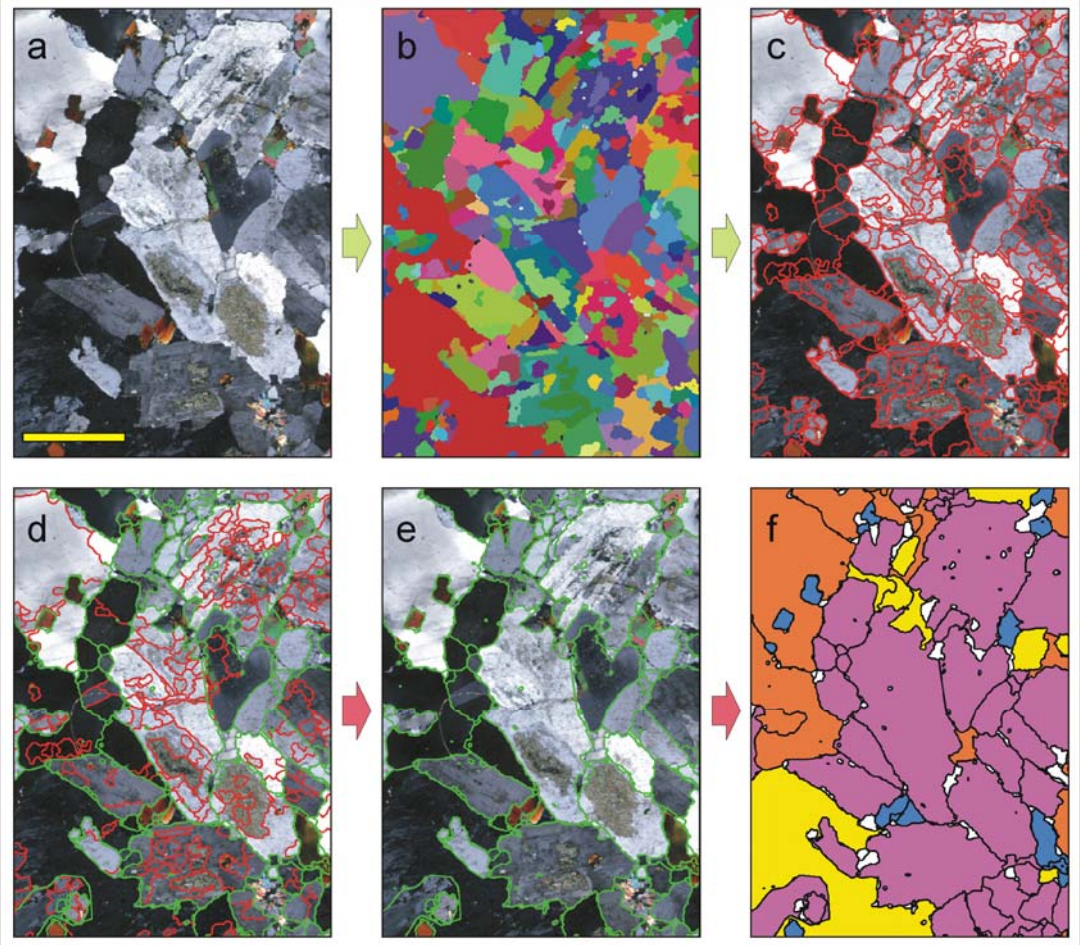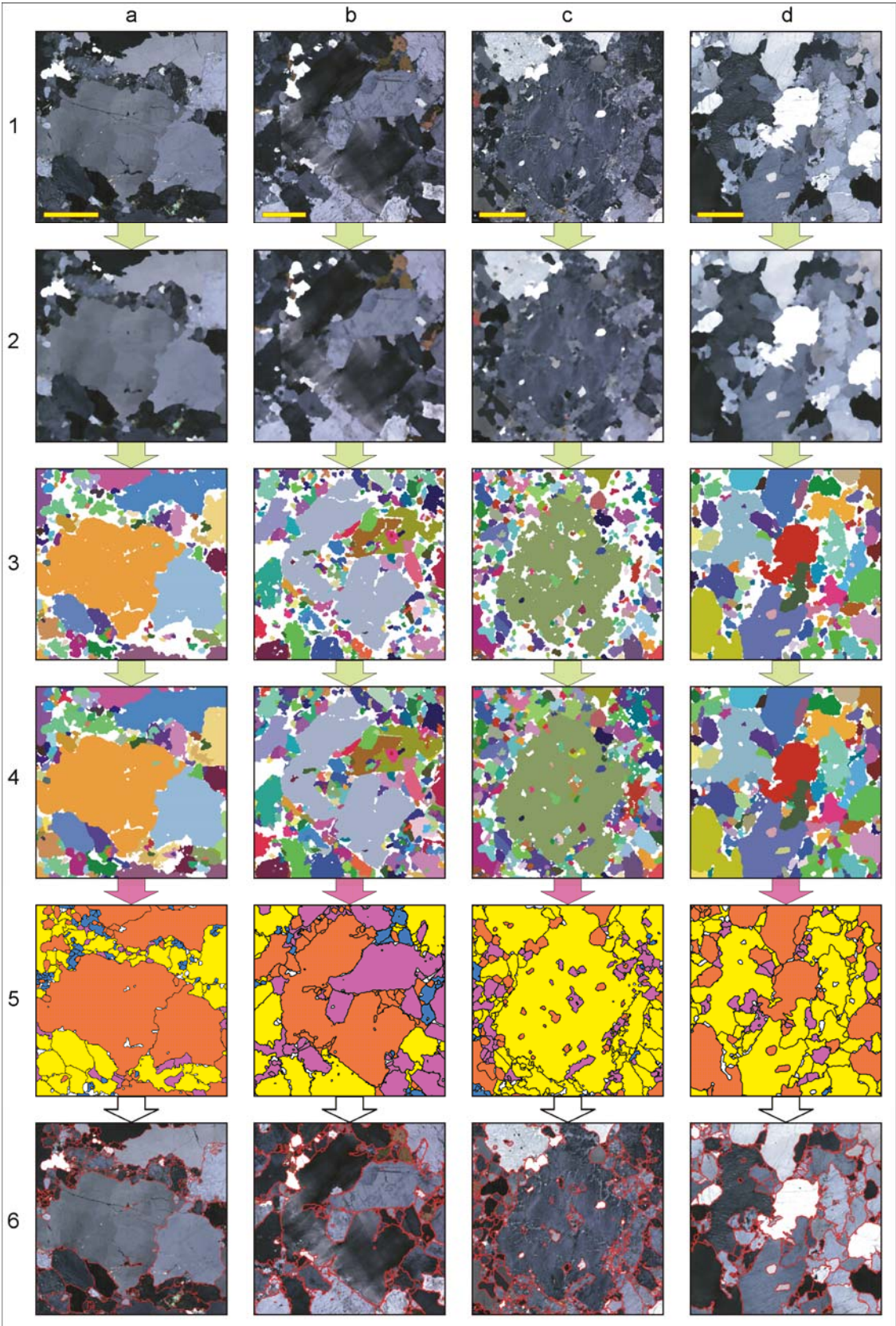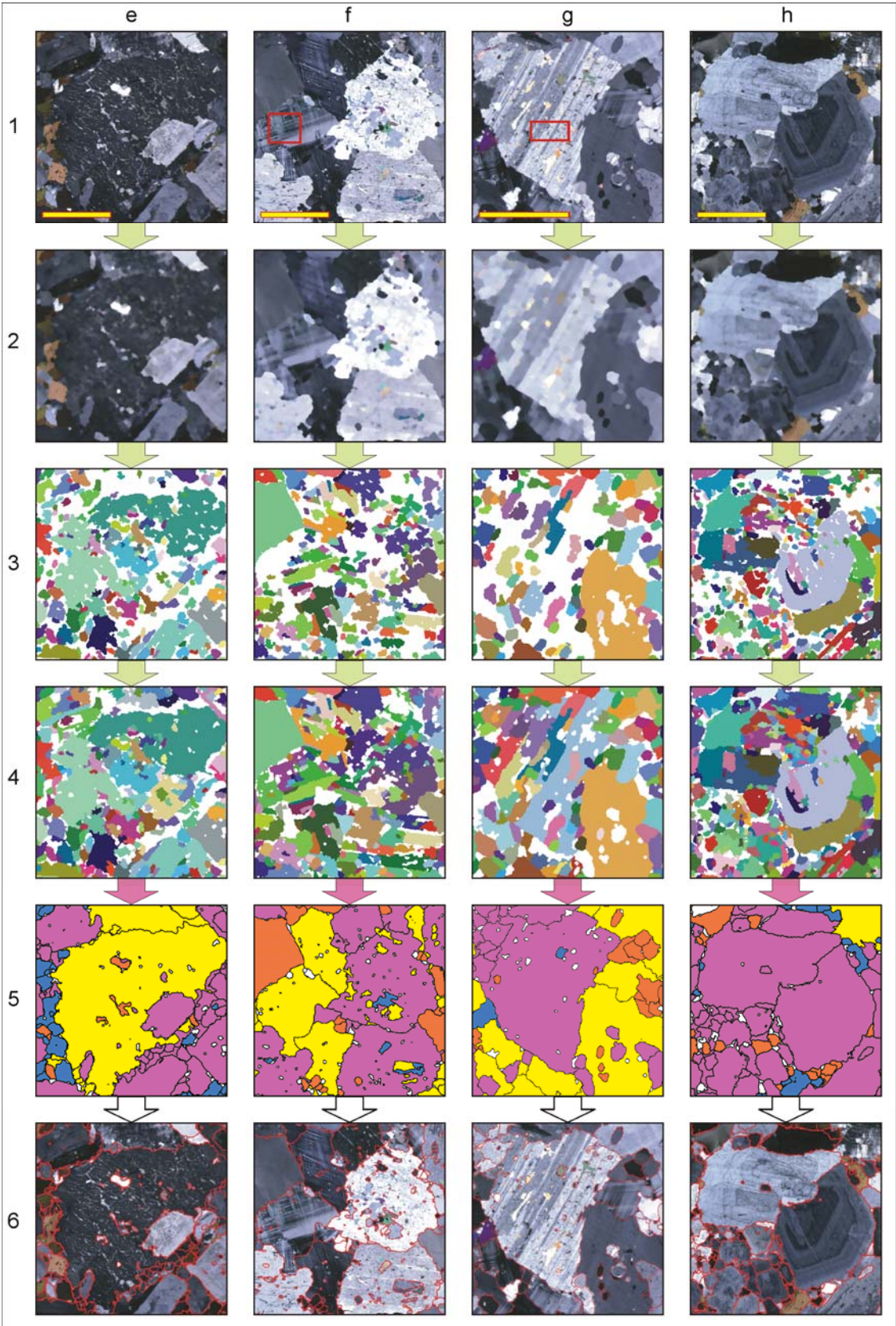
Figure 1

Figure 2

Figure 3
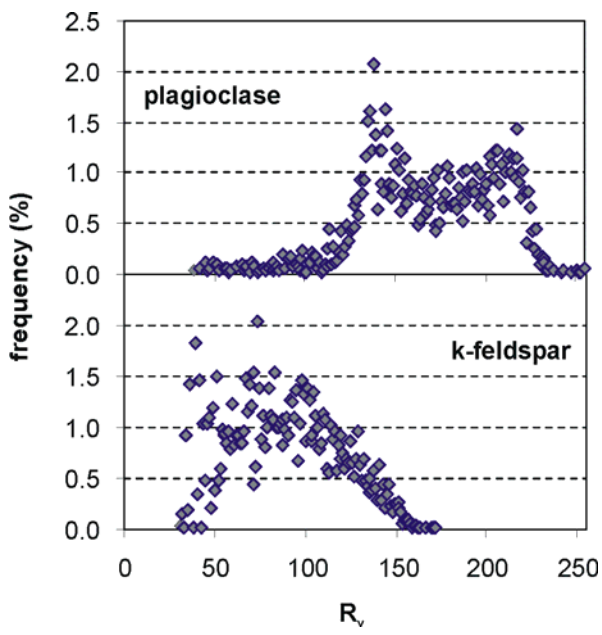
Figure 4

13

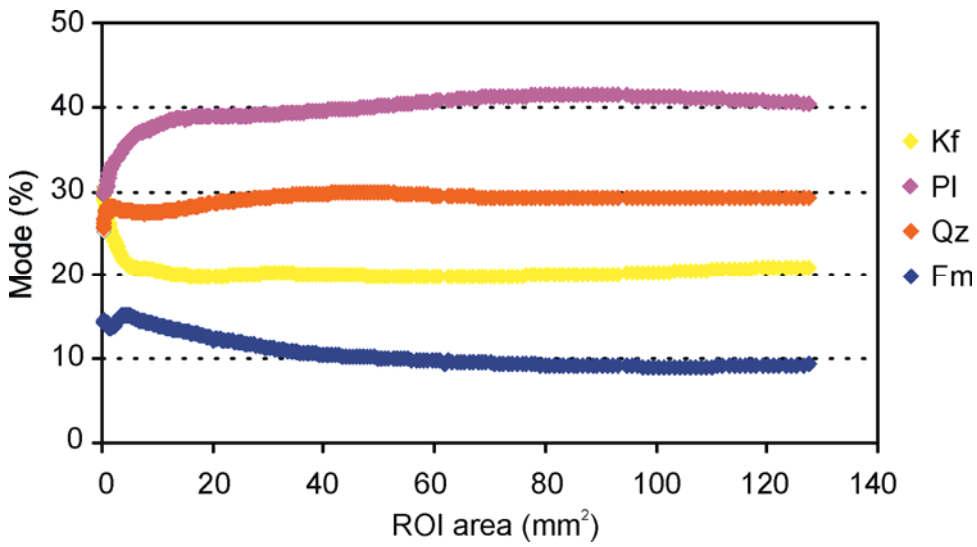Figure 4, continued
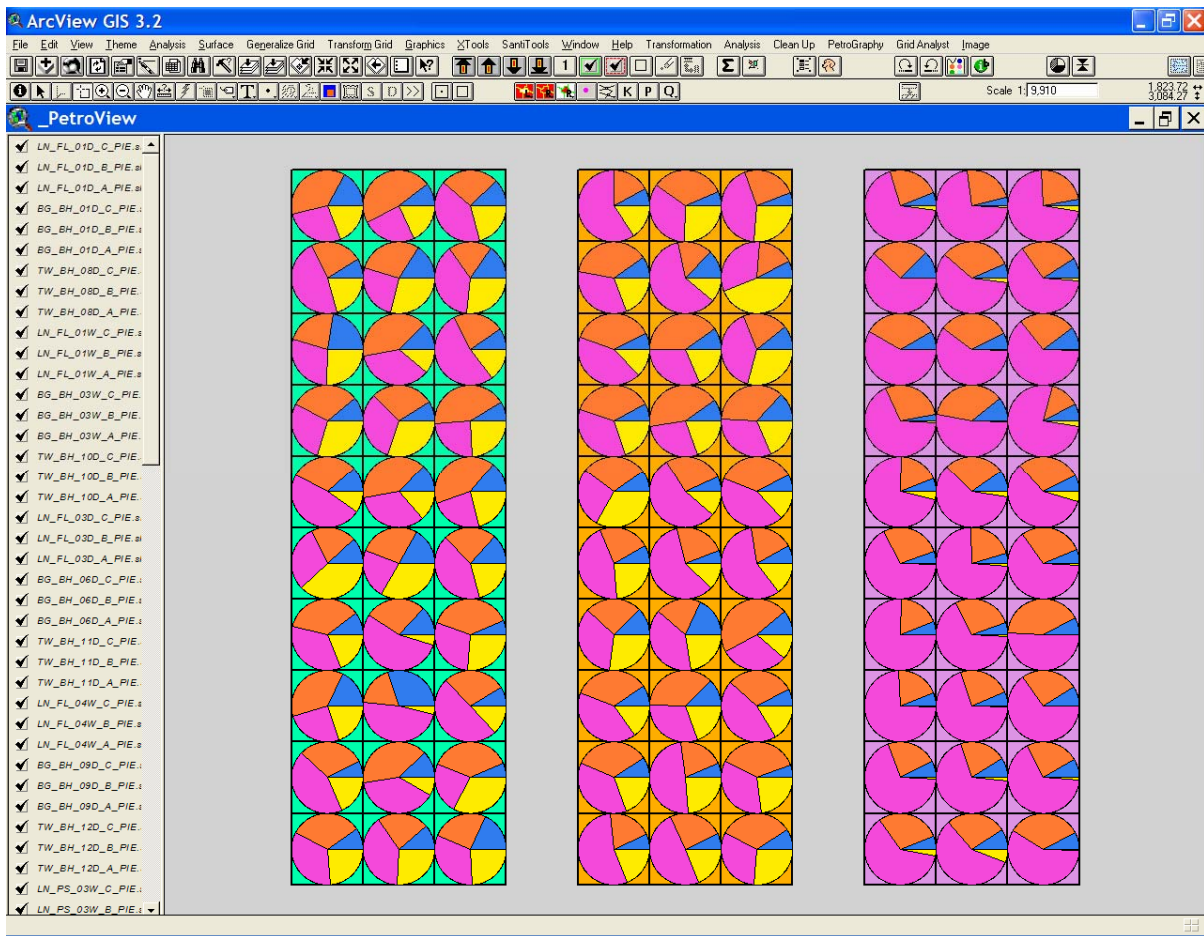
Figure 5

Figure 6

Figure 7

Table 1. input samples. All these rocks are called *granite* in the decorative stone jargon.

Commercial name	Country	Region/State	Petrographic classification	hand samples	thin sections
Desert cream	India	Tamil Nadu	monzo-granite	5	5
Grigio sardo	Italy	Sardegna	monzo-granite	3	9
Yellow topazio	Brasil	Espirito Santo	gneiss	5	15
Golden moon	Brasil	-	gneiss	1	3
Silver cloud	USA	Georgia	monzo-granite	5	15
Barre gray	USA	Vermont	granodiorite	10	30
Lanhelin	France	Bretagne	monzo-granite	10	30
Tolga White	Norway	Hedmark	tonalite	10	30
total number				49	137